Journal of Volcanology and Geothermal Research, 49 (1992) 285–311
Elsevier Science Publishers B.V., Amsterdam

Nonequilibrium flow in volcanic conduits and application to the eruptions of Mt. St. Helens on May 18, 1980, and Vesuvius in AD 79

Flavio Dobran
GNV, Università di Pisa, Via S. Maria 53, 56100 Pisa, Italy
Applied Science Department, New York University, New York, NY 10003, USA

(Received March 4, 1991; revised and accepted July 15, 1991)

ABSTRACT

Dobran, F., 1992. Nonequilibrium flow in volcanic conduits and application to the eruptions of Mt. St Helens on May 18, 1980, and Vesuvius in AD 79. *J Volcanol. Geotherm Res*, 49: 285–311.

A steady-state, one-dimensional, and nonhomogeneous two-phase flow model was developed for the prediction of local flow properties in volcanic conduits. The model incorporates the effects of relative velocity between the phases and for the variable magma viscosity The resulting set of nonlinear differential equations was solved by a stiff numerical solver and the results were verified with the results of basaltic fissure eruptions obtained by a homogeneous two-phase flow model, before applying the model to the eruptions of Mt. St. Helens and Vesuvius volcanoes. This verification, and a study of the sensitivity of several modeling parameters, proved effective in establishing the confidence in the predicted nonequilibrium results of flow distribution in the conduits when the mass flow rate is critical or maximum. The application of the model to the plinian eruptions of Mt. St. Helens on May 18, 1980, and Vesuvius in AD 79, demonstrates the sensitivity of the magma discharge rate and distributions of pressure, volumetric fraction, and velocities of phases, on the hydrous magma viscosity feeding the volcanic conduits. Larger magma viscosities produce smaller mass discharge rates (or greater conduit diameters), smaller exit pressures, larger disequilibrium between the phases, and larger difference between the local lithostatic and fluid pressures in the conduit. This large pressure difference occurs when magma fragments and may cause a rupture of the conduit wall rocks, producing a closure of the conduit and cessation of the volcanic eruption, or water pouring into the conduit from underground aquifers leading to phreatomagmatic explosions The motion of the magma fragmentation zone along a conduit during an eruption can be caused by the varying viscosity of magma feeding the volcanic conduit and may cause intermittent phreatomagmatic explosions during the plinian phases as different underground aquifers are activated at different depths The variation of magma viscosity during the eruptions of Mt St. Helens in 1980 and Vesuvius in AD 79 is normally associated with the tapping of magmas from different depths of the magma chambers This variation of viscosity, which can include different crystal and dissolved water contents, can also produce conduit wall erosion, the onset and collapse of volcanic columns above the vent, and the onset and cessation of pyroclastic flows and surges.

1. Introduction

The discharge of magma from a volcanic system through the country rock can take place through various types of conduits, depending on the type of magma at depth and on the geological and structural characteristics of the overlying rocks and soil. The erupted magma and volcanic surface features provide many clues as to how and over what time eruptions occurred. Thus, very large sheets of lava plateaus are formed when large volumes of low viscosity or basaltic magmas erupt from fissure eruptions. The initial flow through fissures may be sebsequently changed by the closure of small-width fissures due to magma cooling and solidification, and enlargement of large-width fissures due to melting and erosion

NOTATION

A	flow cross-sectional area
B_1, B_2	coefficients in Eqns. (3) and (19)
C_D	drag coefficient
C_{fi}	interfacial friction coefficient
D	conduit diameter
D_H	hydraulic diameter, defined by Eqn. (2)
d	bubble or particle/droplet diameter
F	friction force per unit area
f	friction factor
G	mass flux, M/A
g	gravitational acceleration
h	depth, see Fig. 1
K	entrance loss coefficient
L	conduit length
M	mass flow-rate
N	bubble density
n_o	exponent in solubility law, Eqn. (11)
P	pressure
R	gas constant
Re	Reynolds number
Ri	Richardson number, defined by Eqn. (49)
r_d^*	defined by Eqn. (27)
s	solubility constant in Eqn. (11)
T	temperature
u	velocity
We	Weber number defined by Eqn. (33)
w	fissure half-width
X	exsolved gas mass fraction
$\boldsymbol{X}$	vector of dependent variables, defined by Eqn. (41)
Y	dissolved gas mass fraction
z	distance along a conduit, Fig. 1
α	gas volumetric fraction
μ	viscosity
μ_{Lo}	anhydrous magma viscosity without crystals
μ_o	anhydrous magma viscosity containing crystals
ξ	interfacial drag coefficient
ρ	density
σ	surface tension
Δ	determinant
τ	yield stress
ϕ	crystal volumetric fraction

Subscripts

b	bubble
c	country rock
d	particle/droplet
exit	exit
f	single-phase region
G	gas
H	hydraulic
L	liquid or particle/droplet
m	mean
o	stagnation state in magma chamber
TP	two-phase
w	wall

of country rock, thus forming flows from isolated vents (Bruce and Huppert, 1989). The more viscous silicic magmas erupt pyroclastic products from central vents that may be fed by dikes or magma chambers.

As magma rises through a conduit it exsolves the dissolved gases and it cools, producing a multiphase and multicomponent flow. The cooling of magma is at most 200°C (from the liquidus to the solidus temperature) and is not very significant compared to the magma temperature (about 800°C for rhyolite and 1000°C for basalt), unless the magma interacts with water. This cooling can, however, produce large changes in the physical properties of magma and an isothermal flow consideration in conduits may not always be appropriate. The cooling produces crystallization that leads to an increase of magma viscosity, density, and the dissolved gas content in the liquid. The increase of dissolved gas content in the liquid due to crystallization is largely offset by the decrease due to exsolution. The dissolved gases in the liquid consist primarily of water vapor and carbon dioxide and begin exsolving when the pressure in magma is sufficiently reduced. The exsolved gases form critical nuclei or bubbles which subsequently grow by mass diffusion, inertia, heat transfer, surface tension, and decompression (Sparks, 1978). The crystallization and exsolution processes within a conduit can produce different flow regimes and nonequilibrium effects between the phases under certain combinations of magma withdrawal rate, conduit size, and physical and chemical properties of magma in the magma chamber. A nonequilibrium flow of magma and gas can occur when the bubble growth is prevented by the large magma viscosity, causing an excess pressure buildup between the two phases when the bubbles are very small (several microns). After the magma fragments, the mixture viscosity is greatly reduced and large accelerations and relative velocity increase between the phases can occur due to the gas expansion and reduction of the

interfacial drag. An interaction of magma with the underground aquifers can produce further chemical, mechanical, and thermal nonequilibrium effects.

The modeling of magma flow in volcanic conduits has been performed by the steady, one-dimensional, and homogeneous models (Kieffer, 1977; Pai et al., 1978; Wilson et al., 1980; Wilson and Head, 1981; Buresti and Casarosa, 1989; Giberti and Wilson, 1990), by the steady, one-dimensional, and separated flow model (Vergniolle and Jaupart, 1986), and by an unsteady, one-dimensional, and homogeneous model (Turcotte et al., 1990). The isothermal and homogeneous models of Wilson et al. (1980) and Wilson and Head (1981) were employed to study the motion of magma and gas along conduits with variable area and a given pressure assumed to be lithostatic. Under these conditions the magma pressure at the conduit exit is atmospheric and the flow cross-sectional area exhibits almost a constant shape up to the depth where the local two-phase flow velocity becomes sonic. Beyond this point the flow becomes supersonic and requires an area increase of the conduit. There is an evidence that the exit pressures of pyroclastic products are larger than the atmospheric pressure, and that the flow exiting from a conduit is supersonic and interacting with the local atmosphere through a complex system of shocks (Kieffer, 1981). A nonlithostatic pressure gradient of magma in a conduit allows for the deformation and failure of rocks and is believed to produce violent phreatomagmatic eruptions when the pressure of fragmented magma falls sufficiently below the local lithostatic pressure, since it can cause water from the underground aquifers to flow into the conduit after the wall rupture (Barberi et al., 1988).

An alternate steady-state and homogeneous model which allows for the temperature variation of the gas–particle mixture and which is applicable to the fragmented regime of magma in conduits was proposed by Buresti and Casarosa (1989). For a near-uniform flow cross-sectional area and adiabatic conduit, this model predicts a negligible temperature change of the two-phase mixture. The separated flow model of Vergniolle and Jaupart (1986) allows for the relative velocity between the phases and may be applicable to basaltic magmas with known two-phase flow conditions at the conduit entrance, bubbly flow regime, and low void fractions at the conduit exit. This model predicts that at any location along the conduit the gas volumetric fraction computed by the homogeneous model is larger than the one predicted by the separated flow model, and that the pressure drop of the separated flow model is smaller than the lithostatic pressure drop along a conduit. The homogeneous model of Giberti and Wilson (1990) also predicts a nonlithostatic pressure distribution along the conduits of different shapes, and exit pressures in excess of the atmospheric. By neglecting the weight of the magma column and friction along the conduit wall, Turcotte et al. (1990) applied a transient, one-dimensional, and homogeneous model to the wave propagation along the conduit after a sudden pressure decrease at the conduit exit.

The plinian eruptions of Mt. St. Helens on May 18, 1980, and Vesuvius on August 24 and 25 in AD 79, involved magma withdrawal from deep magma chambers where the magma flow through conduits produced different two-phase flow regimes and interactions with subterranean water (Sigurdsson et al., 1985; Carey and Sigurdsson, 1985). The magmas from these volcanoes contain high silicic contents and may produce large frictional pressure drops in conduits due to their large viscosities. This in turn may produce considerable nonequilibrium effects and invalidate the predictions from homogeneous two-phase flow modeling. These considerations and a need to produce more reliable modeling of two-phase flows in volcanic conduits for the purpose of determining more accurate distributions of pyroclastic dispersions above the volcanic vents and for providing future simulation capabilities of volcanic

eruptions (Dobran et al., 1990) led to the development of the nonequilibrium flow model presented in this paper. This nonequilibrium model allows for the relative velocity between the phases, variable magma viscosity, and for different flow regimes. After being verified with the homogeneous model of basaltic fissure eruptions, the model was applied to the eruptions of Mt. St. Helens in 1980 and Vesuvius in AD 79 for the purpose of determining the effects of magma viscosity and conduit size and length on the eruptive dynamics. The results show that large-viscosity magmas feeding the conduits can produce a significant difference between the local lithostatic and fluid pressure in the conduit when the magma fragments. This pressure difference can cause a failure of the conduit wall and lead to the cessation of the eruption or water inflow into the conduit that can produce phreatomagmatic explosions. Larger-viscosity magmas also produce smaller exit pressures and larger disequilibrium effects in the magma fragmentation region and at the exit of the conduits.

2. Description of the nonequilibrium model

2.1 Single-phase flow region

The flow of magma through a volcanic conduit may be considered to be a quasi steady-state process whereby the magma accelerates from the stagnation state o in the magma chamber and begins exsolving the dissolved gas at a height z_f above the chamber (Fig. 1). In the region from $z=0$ to $z=z_f$, the magma flow can be considered as an effective single-phase fluid with a mean density and viscosity that account for the dissolved gas and crystals present in the liquid. Due to the short transit time of fluid in a conduit (several minutes to hours, or days at most), the crystal content cannot change significantly and a mean value can be used. The single-phase flow length z_f can be easily established by applying a one-dimensional form of the momentum equation (or

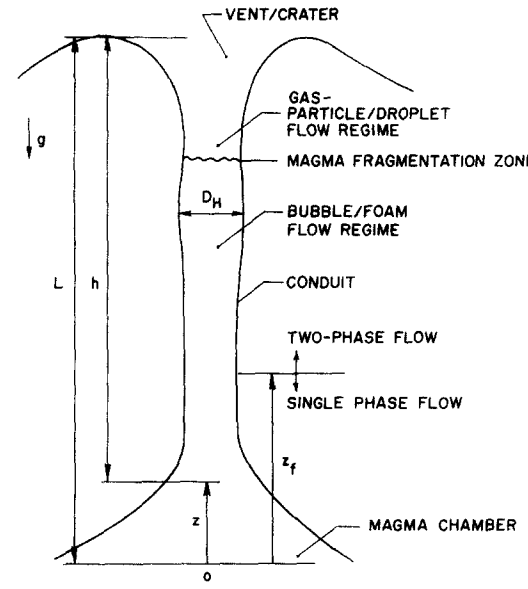

Fig. 1. Schematic illustration of a volcanic conduit of length L and hydraulic diameter D_H. Magma accelerates from the stagnation state o and begins exsolving at $z=z_f$.

Bernoulli equation with friction) between the stagnation state o in the magma chamber and height z_f, i.e.:

$$P_o = P_f + (1+K)G^2/(2\rho_L) + 4(f/D_H)z_f G^2/(2\rho_L) + \rho_L g z_f$$

which gives:

$$z_f = \frac{D_H}{4f}\left[\frac{2\rho_L(P_o - P_f)}{G^2} - 1 + K\right] \times \frac{1}{1+\dfrac{2\rho_L g D_H}{G^2 4f}} \qquad (1)$$

where ρ_L is an effective density of magma, G is the mass flux (mass flow rate of magma per unit area), f is a friction loss coefficient, and D_H is the hydraulic diameter of the conduit which is defined in terms of the flow cross-sectional area A and wetted perimeter ξ_w, i.e.:

$$D_H = 4A/\xi_w \qquad (2)$$

In Eqn. (1) K is the entrance loss coefficient and it ranges from $K=0.03$–0.05 for smooth entrances to $K=0.4$–0.5 for sharp-edged en-

trances (White, 1979). The friction coefficient f depends on the conduit geometry, laminar and turbulent flow, and can be expressed as:

$$f=\frac{B_1}{Re}+B_2, \qquad Re=\frac{GD_H}{\mu_L} \tag{3}$$

where μ_L is an appropriate magma viscosity and Re is the Reynolds number. For a circular conduit and fairly rough walls $B_1=16$ and $B_2=0.01$–0.05, whereas for a fissure $B_1=24$. Equation (3) is obviously an approximation to the actual friction factor behavior and may be viewed as a parameter in the model whose effect on the results must be carefully considered. The magma chamber pressure P_o in Eqn. (1) must be bracketed by the lithostatic pressure of the overlying rocks and soil and the rock yield stress τ_c. At magma chamber depths τ_c is probably limited by 50 MPa due to the plasticity of rocks at great depths induced by the cooling of magma (Wilson and Head, 1981). An appropriate range of values of the stagnation pressure for use in Eqn. (1) is thus:

$$\rho_c gL \leqq P_o \leqq \rho_c gL+\tau_c \tag{4}$$

where ρ_c is the average density of the country rock (about 2700 kg/m^3) and L is the conduit length (see Fig. 1).

Equations (1)–(3), with the assumption of the lithostatic magma pressure distribution, $P_o-P_f=\rho_c g z_f$, can be used to establish the minimum flow velocity of magma through conduits, i.e.:

$$u_{fmin}=\frac{B_1\mu_L}{B_2\rho_L 2D_H}\left\{\left(1+\frac{4B_2\rho_L(\rho_c-\rho_L)8gD_H^3}{(4B_1)^2\mu_L^2}\right)^{1/2}-1\right\} \tag{5}$$

This result is identical to the corresponding result of Wilson and Head (1981), inspite of the neglect of entrance losses and flow acceleration from a stagnation state in their model. The inclusion of the magma yield stress in Eqn. (5) produces smaller flow velocities and is appropriate for magmas close to the solidus temperature.

2.2 Two-phase flow regions

For $z>z_f$ in Figure 1, the fluid flow can be modeled by an effective two-phase flow model that ignores the temperature variation of the mixture and multi-dimensional effects. The one-dimensional approximation will be valid for conduit diameter to length ratios much less than one, and the isothermal nature of the flow will prevail due to the large thermal capacity of magma and in the absence of the mass transfer at the conduit wall, as may be caused by water interacting with magma. For the bubble sizes expected in the bubbly flow regime (greater than several microns), the pressure difference between the phases (Sparks, 1978) can be ignored compared to the pressure level in the conduit, and assuming that the conduit erosion rate is negligible in comparison with the magma discharge rate, the governing two-phase flow equations expressing the balance of mass and momentum can be written as (see Dobran, 1987, for example):

$$M_G=\rho_G\alpha A u_G=XM \tag{6}$$

$$M_L=\rho_{Lm}(1-\alpha)A u_L=(1-X)M \tag{7}$$

$$\rho_G u_G A\alpha\frac{du_G}{dz}=-\alpha A\frac{dP}{dz}-F_{LG}A-F_{wG}A-\rho_G g\alpha A \tag{8}$$

$$\rho_{Lm}u_L A(1-\alpha)\frac{du_L}{dz}=-(1-\alpha)A\frac{dP}{dz}+F_{LG}A-F_{wL}A-\rho_{Lm}g(1-\alpha)A \tag{9}$$

where M is the magma flow rate, u is the velocity, α is the volumetric fraction, X is the exsolved gas mass fraction, and where the subscripts G and L pertain to the gas and liquid (or particle/droplet) phases. In above-equa-

tions ρ_{Lm} is the mean magma density containing the dissolved gas mass fraction Y and is given by:

$$\frac{1}{\rho_{Lm}}=\frac{Y}{\rho_G}+\frac{1-Y}{\rho_L} \tag{10}$$

The dissolved gas fraction Y can be determined from a constitutive equation or an exsolution law of the following form:

$$Y=sP^{n_o} \tag{11}$$

where s and n_o are the parameters expressing different types of magmas. The relation expressed by Eqn. (11) comes from the studies of the permeation of gases through metals (Fast, 1972) and is generally assumed to be valid for silicate melts (Sparks, 1978). It is important to note that Eqns. (6)–(9) are general and can be employed for modeling the bubbly flow before the magma fragments and to gas-particle/droplet flow after the magma fragments (see Fig. 1). The different flow regimes in these equations are specified by the constitutive equations for F_{LG}, F_{wG}, and F_{wL}. F_{LG} accounts for the interfacial drag between the phases, whereas F_{wL} and F_{wG} account for the frictional effects between the magma and conduit wall in the bubbly flow regime (before magma fragmentation) and between the gas and conduit wall in the gas-particle/droplet flow regime (after magma fragmentation), respectively. These drag forces can be expressed as follows (Dobran, 1987):

$$F_{LG}=\xi_{GG}\,(u_G-u_L) \tag{12}$$

$$\begin{aligned} F_{wL}&\neq 0;\ \text{in the bubbly flow regime}\\ &=0;\ \text{in the gas-particle/droplet flow regime} \end{aligned} \tag{13}$$

$$\begin{aligned} F_{wG}&=0;\ \text{in bubbly flow regime}\\ F_{wG}&\neq 0;\ \text{in gas-particle/droplet flow regime} \end{aligned} \tag{14}$$

where the interphase drag coefficient $\xi_{GG}\geqslant 0$.

The exsolved gas fraction X can be computed from the assumptions of no phase change or mass transfer across the conduit wall. Thus:

$$(M_G)_{\text{exsolved}}+(M_G)_{\text{dissolved}}$$

$$\begin{cases} =XM+Y(1-X)M=\text{constant}\\ =X_fM+Y_f(1-X_f)M \end{cases}$$

or

$$X=\frac{X_f+Y_f(1-X_f)-Y}{1-Y} \tag{15}$$

where Y_f is the maximum dissolved gas mass fraction in magma and can be computed from Eq. (11), i.e. $Y_f=sP_f^{n_o}$. With the assumptions of temperature and pressure equilibriums between the phases, the equations of state provide the necessary relations between densities and pressure:

$$\rho_G=\rho_G(T,P),\qquad \rho_L=\rho_L(T,P) \tag{16}$$

for use in the above equations.

The constitutive equations for ξ_{GG}, F_{wL} and F_{wG} must now be specified for the anticipated flow regimes which can prevail in volcanic conduits. For usual fluids, such as a mixture of air and water, the bubbly flow regime occurs at low gas volumetric fractions, or $0\leqslant\alpha\leqslant\alpha_b=0.3$ (Wallis, 1969). For void fractions between about 0.3 and 0.8 the two-phase flow is transitional or in the churn/turbulent regime with large distortions of bubbles intermittently occupying the entire flow cross-section of the channel. For void fractions greater than about 0.8, the bubble agglomeration produces a transition to the annular flow regime where a liquid film flows adjacent to the channel wall and the gas with dispersed droplets occupies the central core (Wallis, 1969). The silicate liquids do not appear, however, to behave as the normal fluids as described above, probably due to the large magma viscosity which prevents relative motion between the phases. These liquids maintain the bubbly or foamy flow regime up to a volumetric fraction of about 0.75 (Sparks, 1978) where the high packing density of bubbles leads to the magma fragmentation. In the fragmented magma flow regime the gas

forms a continuous phase and is in contact with the conduit wall, with the particles and droplets of magma being dispersed in the flow and dragged along by the expanding gas phase.

The constitutive equations for nonsilicate fluids are reasonably well understood for the bubbly gas-particle flow regimes (Wallis, 1969; Ishii and Zuber, 1979; Dobran, 1987), and need to be extrapolated to magmas. The maintenance of the foamy flow regime up to the magma disruption at $\alpha=0.75$ implies that in the proximity of this region the two-phase flow viscosity has to be very large (bubble packing or locking viscosity) which is able to produce a large fluid frictional pressure drop. As further discussed below, the magma viscosity also increases due to exsolution, implying that it should be unreasonable to assume a constant magma viscosity in the bubbly flow regime. The general constitutive relations applicable to either bubbly or gas-particle flow regimes can be expressed as follows (Dobran, 1987):

$$\xi_{GG}=\frac{2C_{f_i}}{D_H}\alpha^{1/2}\rho_G|u_G-u_L| \tag{17}$$

$$F_{wL},F_{wG}=\frac{2f_{TP}G^2}{D_H\rho_m} \tag{18}$$

$$f_{TP}=\frac{B_1}{Re}+B_2, \qquad Re=\frac{GD_H}{\mu_m} \tag{19}$$

$$\rho_m=\alpha\rho_G+(1-\alpha)\rho_{Lm} \tag{20}$$

where for:

Bubbly flow regime: $0\leqslant\alpha\leqslant 0.75$

$$C_D=\frac{24}{Re_b}(1+0.15\,Re_b^{0.687}),\ Re_b\leqq 1000 \tag{21}$$

$$C_D=0.44,\ Re_b>1000$$

$$C_{D_{1-\alpha}}=C_D\,(1-\alpha)^{-4.7} \tag{22}$$

$$Re_b=\frac{\rho_L d_b(1-\alpha)|u_G-u_L|}{\mu_m} \tag{23}$$

$$d_b=\left(\frac{6\alpha}{\pi N}\right)^{1/3}$$

$$\mu_m=\mu_L\,(1-\alpha)^{-2.5(\mu_G+0.4\mu_L)/(\mu_G+\mu_L)} \tag{24}$$

$$C_{f_i}=\frac{3}{8}C_{D_{1-\alpha}}\,(1-\alpha)^3\,(\alpha)^{1/2}\frac{\rho_L D_H}{\rho_G d_b} \tag{25}$$

$$F_{wG}=0 \tag{26}$$

Gas-particle/ droplet flow regime: $0.75<\alpha<1$

$$\left.\begin{aligned} &C_D=\frac{24}{Re_d}\,(1+0.1Re_b^{0.75})\\ &r_d^*=\frac{d_d}{z}\left(\frac{\rho_G g(\rho_L-\rho_G)}{\mu_G^2}\right)^{1/3}<34.65\\ &C_D=0.45\left(\frac{1+17.67[f(1-\alpha)]^{6.7}}{18.67\,f(1-\alpha)}\right)^2\\ &r_d^*\geqq 34.65\\ &f(1-\alpha)=\alpha^{1/2}\frac{\mu_G}{\mu_m} \end{aligned}\right| \tag{27}$$

$$C_{f_i}=\frac{3}{8}\frac{1-\alpha}{\alpha^{1/2}}\frac{D_H}{d_d}C_D \tag{28}$$

$$\left.\begin{aligned} &d_d=\frac{4\sigma}{(\sigma g(\rho_L-\rho_G))^{1/2}}\\ &Re_d=\frac{\rho_G d_d|u_G-u_L|}{\mu_m} \end{aligned}\right| \tag{29}$$

$$\mu_m=\mu_G\left(1-\frac{1-\alpha}{\alpha_{dm}}\right)^{-2.5\,\alpha_{dm}(\mu_L+0.4\mu_G)/(\mu_L+\mu_G)} \tag{30}$$

$$\alpha_{dm}=0.62(\text{maximum particle packing density}) \tag{31}$$

$$F_{wL}=0 \tag{32}$$

For most practical applications involving nonsilicate liquids, the drag law for a fluid-particle system can be approximated by that for a solid-particle system, up to a certain particle

size. Beyond this size, the distortion of particle shape and irregular motions become pronounced (Ishii and Zuber, 1979). The use of mixture viscosities in evaluating the viscous drag at the wall and the drag coefficients of bubbly and gas–particle flow regimes is due to the fact that when bubbles or particles more through a fluid they distort the flow field and the motion of particles is affected by other particles imposing forces on the original bubbles and particles. As a result of the additional stresses, the original particles see an increase of resistance to their motion which appears as if it arises from an increased viscosity. Consequently, in analyzing the motion of the suspended particles or evaluating the frictional loss at the wall due to the mixture of fluid and particles, the mixture viscosity should be used. The use of solid particle drag law for $Re_b > 1000$ in Eqn. (21) for bubbly flow is due to the assumption that the exsolved bubbles in magmas are very small or the suspension is foamy, even at relatively large volumetric gas fractions α, and that the bubbles do not significantly distort this flow regime. The transition from the viscous flow regime, where the Reynolds number dependence on C_D is important, to the Newton's regime, where C_D is independent of Re, in the solid particle system is expressed by r_d^* as shown by Eqn. (27). The above drag laws involving the mixture viscosity μ_m have been tested over a wide range of conditions in nonsilicate systems (Ishii and Zuber, 1979) and are sufficient up to the foam or dense packing regimes, with the particle concentrations ranging from 0.5 to 0.99 for both bubbly and droplet flows.

The use of mixture viscosity and the assumption of the bubbly or foamy flow up to the volumetric gas fraction of $\alpha = 0.75$ produces a four-fold increase of viscosity of the mixture, without accounting for the dramatic magma viscosity increase by an order of magnitude with a decrease of water content (see Eqn. 47 below). An appropriate form of the magma viscosity μ_L for use in Eqns. (24) and (30) may be that as expressed by Eqn. (47) or by an alternate power law.

The bubble density N in Eqn. $(23)_2$ depends on the nucleating characteristics of the silicate liquids. For steam–water systems $N = 10^{11}$ m^{-3} and its variation several orders of magnitude from this value does not affect the predicted results of the nonequilibrium two-phase critical flows in tubes (Dobran, 1987). For silicate liquids, the effect of this variation can also be established *aposteriori* as described below. The particle/droplet diameter d_d in Eq. (29) is based on a result whereby a nonsilicate liquid desintegrates to droplets at a critical Weber number of 8 (Ishii and Zuber, 1979), i.e.:

$$We = \frac{\rho_L d_d}{\sigma}\left(\frac{4\sigma g(\rho_L - \rho_G)}{\rho_L^2}\right)^{1/2} = 8 \qquad (33)$$

Taking, for example, a basalt with $\rho_L = 2700$ kg/m^3 and $\sigma = 0.4$ N/m gives $d_d = 20$ mm, and from Eqn. $(23)_2$ $N = 6(0.75)/\pi d_d^3 = 10^5$ m^{-3}. This particle size is consistent with the size of pyroclasts from the plinian eruptions of Mt. St. Helens in 1980 and Vesuvius in AD 79 (Carey and Sigurdsson, 1987; Carey et al., 1990). It should be noted, however, that plinian eruptions generate a spectrum of particle sizes from submicrons to centimeters in size and that a more appropriate way to model this particle spectrum would be by a model consisting of several phases with each particle phase having a unique particle size. The above Weber number criteria supplying the particle/droplet size after magma fragmentation comes from the studies of nonsilicate two-phase flow systems and can at best supply only a *mean* value of d_d. After the magma fragments and the gas expands to high velocities, the relative velocity between the gas and particles will produce further particle fragmentation and production of the fine particles as evidenced in the plinian eruptions. To describe this particle fragmentation requires the consideration of boundary layer or instability stripping mechanisms which is beyond the present modeling objectives, but it may be necessary to consider in the future or

more complicated modeling of gas-particle/droplet flow after magma fragmentation in volcanic conduits. Such a study may produce a lower relative velocity between the phases, since a part of the gas kinetic energy may have to be used for the production of small size pyroclasts.

The initial conditions for the two-phase flow model described above are determined by first locating the position z_f in the conduit and the state of magma at this position. This position can be determined from Eqn. (1) for a given stagnation pressure P_o of magma in the magma chamber and the dissolved gas mass fraction Y_f. The latter information can be used in the exsolution law Eqn. (11) to find the pressure P_f for use in Eqn. (1). The magma mass flux G is assumed to be given, or if the maximum is sought it can be calculated as described below. The conduit diameter is assumed to be known or specifiable, i.e. $D_H = D_H(z)$. Differentiating Eqns. (6) and (7) with respect to z and adjoining them to Eqns. (8) and (9) produces a system of four simultaneous nonlinear ordinary differential equations. These equations, together with Eqns. (10)–(33), can then be used to solve for α, P, u_G, and u_L as functions of z along the conduit, given the initial values of α_f, P_f, u_{Gf}, and u_{Lf}. These initial variables can be computed as follows:

(1) With a given nucleation site density N and diameter of critical nuclei d_f for bubble growth, the initial volume fraction is found from Eqn. $(23)_2$, i.e.:

$$\alpha_f = \frac{\pi}{6} N d_f^3 \tag{34}$$

The nucleation site density and diameter of critical nuclei have the approximate values of $N = 10^{11}$ m^{-3} and $d_f = 50$ μm (Sparks, 1978; Dobran, 1987). This is further justified below in section 3.1 where a parametric study is carried out.

(2) The initial pressure P_f is determined from Eqn. (11) from the knowledge of the type of magma and maximum dissolved gas mass fraction Y_f. Thus:

$$P_f = \left(\frac{Y_f}{s}\right)^{1/n_0} \tag{35}$$

(3) The initial gas velocity u_{Gf} is found from Eqns. (6), (11), and (15), i.e.:

$$u_{Gf} = \frac{X_f G}{\alpha_f \rho_G(T, P_f)} \tag{36}$$

with X_f being determined from Eqns. (6) and (7) with the assumptions of no-slip between the phases, i.e.:

$$X_f = \frac{1}{1 + \dfrac{\rho_L(T,P_f)}{\rho_G(T,P_f)} \dfrac{1-\alpha_f}{\alpha_f}} \tag{37}$$

The no-slip assumption between the phases when the bubble size is critical is an excellent assumption (Dobran, 1987) and is more valid for higher viscosity fluids which impede the relative motion between the phases.

(4) The initial magma velocity u_{Lf} is found from:

$$u_{Lf} = u_{Gf} \tag{38}$$

because of the above no-slip assumption.

The magma density ρ_L does not vary significantly with pressure or dissolved gas content Y, since Y is less than a few percent for all known magmas. The gas density varies, however, significantly along a conduit due to pressure decrease, and the simplest equation of state that may be used is that of a pefect gas whereby:

$$\rho_G = \frac{P}{RT} \tag{39}$$

where R is the gas constant of the exsolved gas (water vapor in the cases considered here). For magma temperatures on the order of 1000°C, the perfect gas law approximation is a very reasonable one.

2.3 Solution procedure of the modeling equations

Equations (6)–(9) can be transformed into the following system of nonlinear ordinary differential equations:

$$A\frac{dX}{dz}=B \tag{40}$$

where X is a vector of the dependent variables, i.e.:

$$X=(\alpha, P, u_G, u_L)^T \tag{41}$$

and where the coefficients of the matrix A and vector B depend on the dependent variables. The solution of the system of equations (40) can then be accomplished with the initial conditions specified by Eqns. (34), (35), (36), and (38) in terms of the conduit flow cross-sectional area $A(z)$, conduit length L, magma conditions in the magma chamber (pressure, temperature, dissolved gas content), physical properties of magma and dissolved gas, and the mass flow rate $M=GA$.

Equation (40) also admits a critical or maximum flow-rate M or mass flux G. This critical flow is determined by satisfying the following necessary and sufficient conditions (Dobran, 1987):

$$\Delta=0 \quad \text{and} \quad n_i=0, \qquad i=1,....,4 \tag{42}$$

where $\Delta=\det(A)$ is the determinant of A, and n_i is the determinant obtained by replacing the ith column of A by the column vector B. The critical flow in a conduit is then obtained by searching for that value of the mass flow-rate M which will yield the conditions specified by Eqn. (42) at the end of the conduit when the conduit flow cross-sectional area is constant.

The numerical solution of the system of differential equations (40) is complicated by the stiffness of these equations in the bubbly flow regime, which required the implementation of a stiff numerical solver (Hindmarsh, 1983) with an absolute error tolerance of 10^{-9}. This produced very accurate solutions and maximum errors of 10^{-3}% in the local mass flow-rates.

3. Results

The nonequilibrium model described in the previous section was first applied to the prediction of flow properties pertaining to basaltic fissure eruptions where the results can be compared with the existing results obtained by a homogeneous flow model. This comparison also required a study of the sensitivity of the model parameters N and d_f to ascertain the confidence limits in the model. After this comparison, the nonequilibrium model was employed to study the plinian eruptions of the Mt. St. Helens on May 18, 1980, and of Vesuvius on August 24 and 25, in AD 79. The predicted results pertain to uniform width fissures and constant diameter conduits and do not account, therefore, for the flarring of volcanic vents.

3.1 Fissures of uniform width

For a fissure of width 2w and length $L \gg w$, the hydraulic diameter $D_H=4w$ according to Eqn. (2), whereby in Eqn. (3) $B_1=24$ and B_2 can be assumed as 0.01. To compare the model's predictions with previous calculations using a homogeneous model an alternate expression for the single phase flow length z_f must be used from that as given by Eqn. (1). This length is found by integrating the single phase flow momentum equation:

$$\rho_{Lm}u\frac{du}{dz}=-\frac{dP}{dz}-\rho_{Lm}g-F_{wL} \tag{43}$$

from $z=0$ where $P=P_o$ to $z=z_f$ where $P=P_f$, and employing the conservation of mass equation:

$$M=\rho_{Lm}uA=\text{constant}=GA \tag{44}$$

and the wall frictional force as determined from Eqn. (18), i.e.:

$$F_{wL}=\frac{2G^2}{D_H\rho_{Lm}}\left(\frac{B_1}{Re}+B_2\right), \qquad Re=\frac{GD_H}{\mu_L} \tag{45}$$

Thus setting $\rho_{Lm}=\rho_L$, since $Y\ll 1$, gives $u=$constant from Eqn. (44) and an integration of Eqn. (43) produces the following result for the single-phase length z_f:

$$z_f=\frac{2w\rho_L(P_o-P_f)}{B_2G^2\left(1+\dfrac{B_1\mu_L}{4wGB_2}+\dfrac{\rho_L g 2w\rho_L}{B_2G^2}\right)} \tag{46}$$

Equation (46) differs from Eqn. (1) in that the former equation ignores the acceleration of magma from the stagnation state in magma chamber and the frictional losses at the conduit entrance.

For a basaltic magma, the appropriate values of the solubility constants are $s=6.8\times10^{-8}$ $Pa^{-0.7}$ and $n_o=0.7$ (Wilson and Head, 1981), whereas the initial bubble diameter and bubble density can be chosen as 50 μm and 10^{11} m^{-3}, respectively (Sparks, 1978; Dobran, 1987). Using also the magma properties: $\sigma=0.36$ N/m, $\rho_{Lm}=2600$ kg/m^3, $T=1200$ K, $Y_f=0.01$, and constant magma viscosities $\mu_L=100$ and 1000 Pa-s, Figure, 2 illustrates the results for the critical discharge rates or mass fluxes and the corresponding values of exit pressure and velocities for fissures of different widths $2w$. The magma chamber pressure P_o used for producing these results was determined form $P_o=\rho_c gL+P_{atm}$, where $\rho_c=2800$ kg/m^3 is the density of country rock, $L=1000$ m is the fissure length, and $P_{atm}=0.1$ MPa is the atmospheric pressure. Moreover, it was also assumed that magma fragments at $\alpha=0.75$ and that no gas exsolution takes place after magma fragmentation.

Figure 2 illustrates the results obtained by the nonhomogeneous model and by the same model when it is assumed that the interfacial drag ξ_{GG} is very large to prevent the relative motion between the phases (the homogeneous flow limit). The triangles and squares in the figure correspond to the computations of Giberti and Wilson (1990) who used the homogeneous model of Wilson et al. (1980) and Wilson and Head (1981) without assuming that the pressure distribution is lithostatic. The first observation in Figure 2 is that the calculations of the present model in the limit of homogeneous flow agree with previous calculations of a homogeneous model which utilizes single-fluid momentum and mass balance equations with effective properties for a two-phase mixture. An increase in fissure width and decrease of magma viscosity have the effect of increasing both the fissure mass flow rates and exit pressures, with only a slight increase of the exit velocity when the flow is assumed to be homogeneous. The effect of large magma vis-

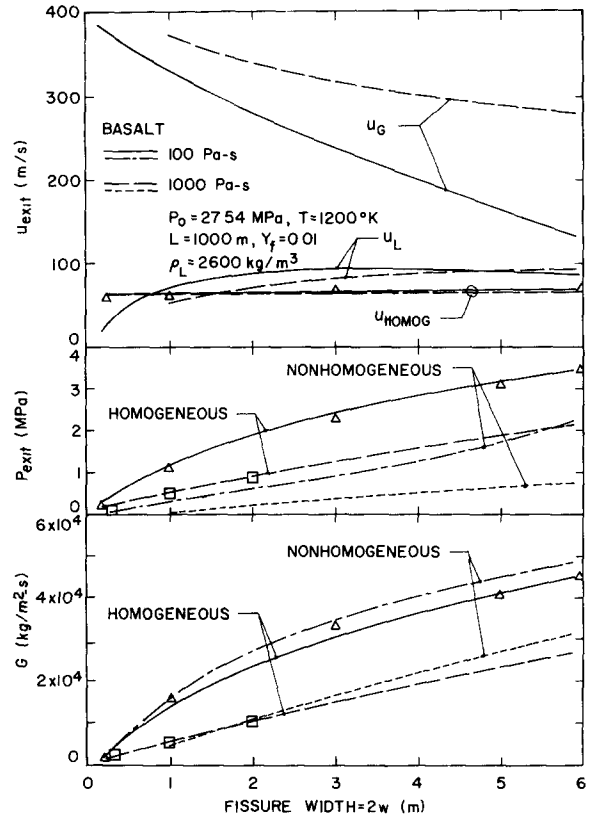

Fig. 2. Distributions of critical discharge rates, exit pressures, and exit velocities for fissures of different widths and magma viscosities, obtained by the nonequilibrium model. The triangles △ (100 Pa-s) and squares □ (1000 Pa-s) pertain to the homogeneous model results of Giberti and Wilson (1990).

cosity is very significant for it reduces considerably the exit pressure and mass flow rate in a constant fissure width when compared with a small viscosity magma. The effect of relative velocity between the phases (nonhomogeneous or nonequilibrium flow) is to affect dramatically the exit pressures and velocities and not to affect significantly the magma flow rates which are generally higher. A more pronounced exit pressure decrease due to the nonequilibrium flow implies that the homogeneous model is inadequate to model small fissure widths because the exit pressure reaches sooner the atmospheric pressure. When this occurs, the exit flow will adjust itself to match the atmospheric conditions. The decreasing fissure widths also produce increasing relative velocities between the phases. Whereas the particle/droplet velocities remain close to the homogeneous values, the gas velocities can be very high (several hundred meters per second) and may be responsible for the lava fountain effect commonly observed in basaltic eruptions (Macdonald, 1972). This result thus shows that it is not necessary to have an annular flow pattern in the fragmented magma regime which is thought to be responsible for the production of high gas velocities which cause the lava fountains (Sparks, 1978; Vergniolle and Jaupart, 1986).

The distributions of volumetric fraction, pressure, and gas and particle/droplet velocities along the conduits of widths $2w=3$ m and $2w=1$ m are shown in Figures 3–6. The abrupt change of the bubbly flow regime to the gas-particle/droplet regime at $\alpha=0.75$ is reflected in different distributions of volumetric fraction, pressure, and velocities in the two regions. In the bubbly flow regime the flow is nearly homogeneous as reflected by similar volumetric fraction, pressure, and velocity distributions. In the fragmented magma regime, however, there is a considerable disequilibrium between the phases which increases with magma viscosity and decreasing fissure width. For a large fissure width and low viscosity

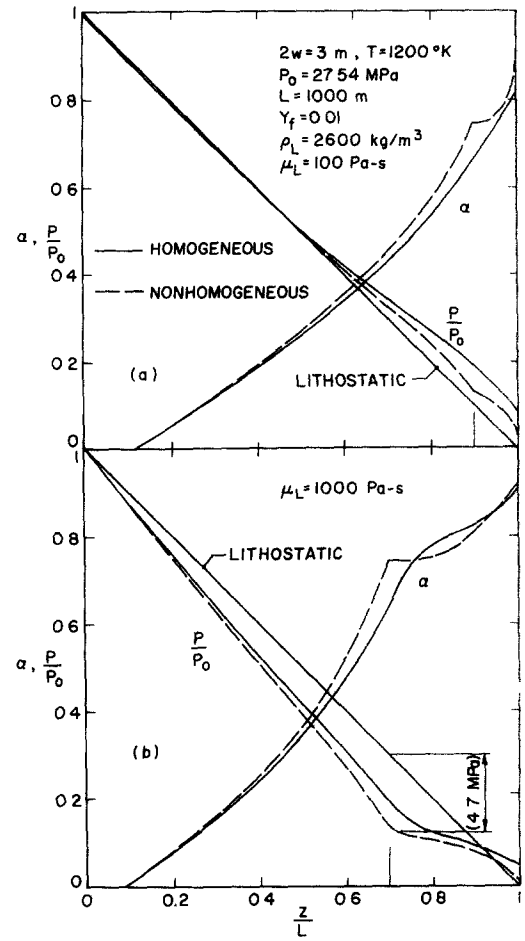

Fig. 3. Distributions of volumetric fraction and pressure along a fissure three meters wide and comparison from the homogeneous and nonhomogeneous modeling. (a) magma viscosity is 100 Pa-s, and (b) magma viscosity is 1000 Pa-s.

magma, the fluid pressure exceeds the lithostatic pressure along the entire length of the conduit (Fig. 3a), whereas for a high-viscosity magma, which causes a large frictional pressure drop, the pressure is reduced below the lithostatic pressure along most of the conduit and exceeds the latter only near the conduit exit (Fig. 3b). The fluid pressure decrease below the lithostatic is especially pronounced for small fissure widths (Fig. 5b), indicating the possibility of rock fracture and water pouring into the conduits from underground aquifers. The flow of water into conduits and mixing

with fragmented magma is advocated by Barberi et al. (1988) as the most likely cause of the phreatomagmatic explosions. The results of the present modeling effort appear to confirm this conclusion.

The velocity distributions in Figures 4 and 6 show that after magma fragmentation there is some delay in accelerating the particle/droplet phase which has a much greater inertia than the gas phase which rapidly expands. In the bubbly flow regime the high viscosity of magma impedes the relative motion between the phases and there is an enormous reduction in the interfacial drag between the phases as the magma fragments. While all the homogeneous flow exit pressures in Figures 2, 3 and 5 are greater than atmospheric, this is not the case for the nonhomogeneous flow with $\mu_L = 1000$ Pa-s and $2w = 1$ m as shown in more detail in the insert to the right of Figure 5b. This result

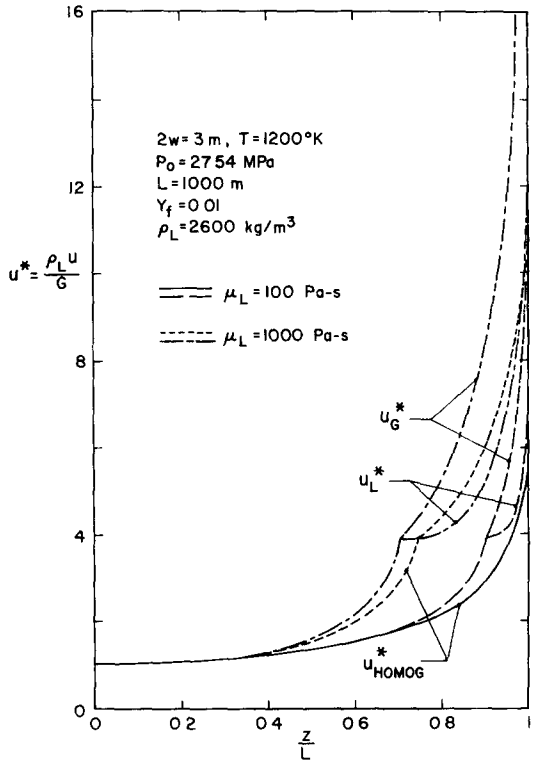

Fig. 4. Distributions of velocities along a fissure three meters wide for different magma viscosities and comparison from the homogeneous and nonhomogeneous modeling.

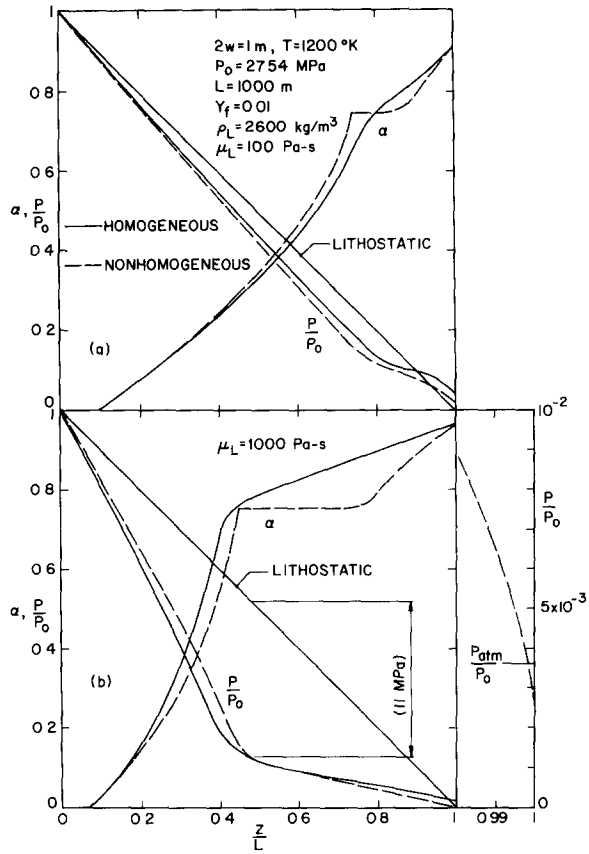

Fig. 5. Distributions of volumetric fraction and pressure along a fissure one meter wide and comparison from the homogeneous and nonhomogeneous modeling. (a) magma viscosity is 100 Pa-s, and (b) magma viscosity is 1000 Pa-s.

clearly shows that such a flow cannot occur with $P_{atm} = 0.1$ MPa and that it would have to adjust itself to produce a subcritical flow condition such that the exit pressure is nearly balanced with the atmospheric pressure.

The effect of the bubble density N and size of the critical nuclei d_f for bubble growth on the above results was investigated by varying these parameters from $d_f = 10$–100 μm and $N = 10^9$–10^{11} m^{-3}. This variation produces maximum changes of $\pm 10\%$ of the critical discharge rates and pressures and $\pm 1\%$ in the exit velocities and volumetric fractions for the range of fissure geometries and magma properties considered above. In general, increasing values of d_f produce larger critical flows and

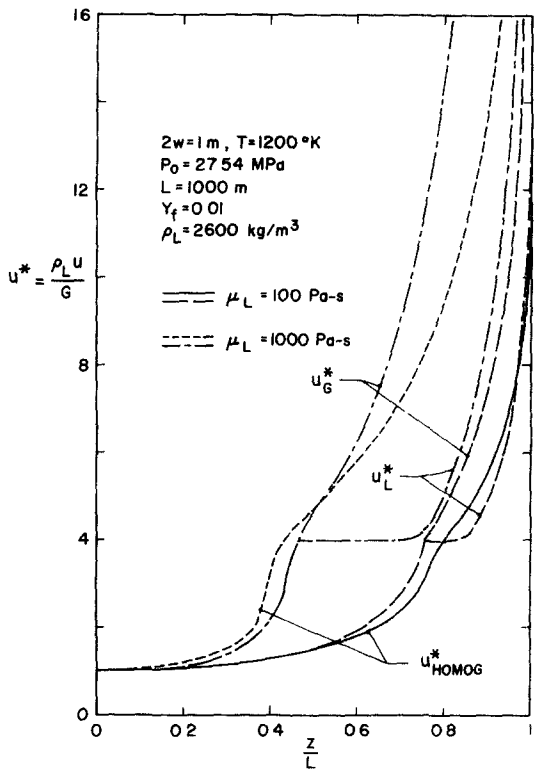

Fig. 6. Distributions of velocities along a fissure one meter wide for different magma viscosities and comparison from the homogeneous and nonhomogeneous modeling.

exit pressures, whereas smaller N produce smaller critical flows and exit pressures, with all other parameters being the same. Moreover, the most significant effects produced by the changes of d_f and N on the critical flows occur at smaller fissure widths where nonequilibrium effects are largest. The values of $d_f = 50$ μm and $n = 10^{11}$ m^{-3} used in the calculations thus appear to be adequate and are, moreover, consistent with the previous studies (Sparks, 1978; Dobran, 1987). Sparks (1978) notes that d_f is larger than 5 μm as ascertained from pumice and scoria fragments.

3.2 The eruption of Mt. St. Helens on May 18, 1980

The nonequilibrium model of section 2 can be used to explain the shifts of the eruption styles during the May 18, 1980 eruption of Mt. St. Helens. The column height variations and mass balance calculations based on the volumes of pyroclastic flows and ash show that shortly after the blast/surge event at 09.00 hrs on May 18, 1980 a plinian column began forming over Mt. St. Helens and lasted until noon during which time a mafic dacite was emptied from a magma chamber at a rate of about 2×10^7 kg/s. From about noon to 16.00 hrs the eruption rate increased to 4.4×10^7 kg/s and was caused by the eruption of a denser silicic andesite. This eruption phase also produced pyroclastic flows due to the eruption column collapse. For the subsequent two hours the plinian activity was reestablished with a diminished eruption rate of about 10^7 kg/s (Carey et al., 1990).

The early plinian phase activity is associated with tapping of a mafic dacite from the upper regions of the magma chamber, whereas the increased rate of erupted mass during the intermediate phase is associated with tapping of a lighter and less viscous silicic andesite from the lower regions of the magma chamber (Fig. 7). The second plinian activity during the last phase of eruption is associated with tapping of a mixture of mafic dacite and silicic andesite from the chamber. These erupted mass fluxes can be very well correlated with the varying magma viscosity feeding the volcanic conduit of the Mt. St. Helens.

The data in Table 1 were compiled from several sources and can be used to determine the necessary parameters for the input into the model. These data involve a maximum dissolved water content in magma of $Y_f = 4.6\%$, magma density of $\rho_{Lm} = 2600$ kg/m^3, magma temperature of $T = 1200$ K, an estimated hydrous magma viscosity from 10^5 to 10^6 Pa-s that also contains about 40% crystals by volume, a confining magma pressure $P_o = 185$–265 MPa computed from the country rock density $\rho_c = 2700$ kg/m^3 and conduit lengths $L = 7$–10 km, a conduit diameter of 95 m, a volumetric fraction of about 0.75 at the onset of magma fragmentation, and a dacitic magma discharge

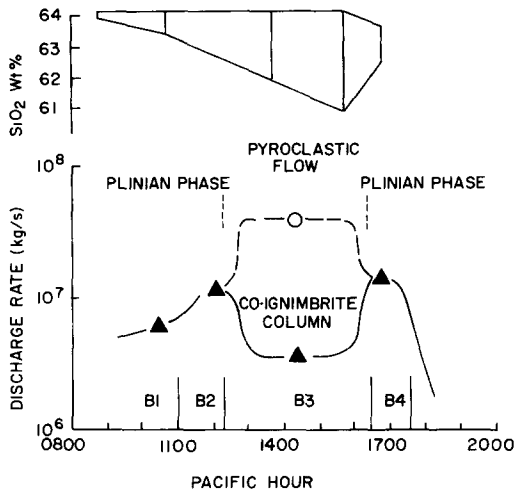

Fig. 7 Variation of magma discharge versus time during the eruption of Mt. St. Helens on May. 18, 1980. Solid triangles represent magma discharge calculated from the model-based column height estimates. The dashed curve represents the average magma discharge based on the volume of pyroclastic flows and co-ignimbrite ash. At the top of the figure the compositional variation of erupted products is shown as a function of time. After Carey et al. (1990).

of about 2×10^7 kg/s during the plinian phases. Based on these data the nonequilibrium model of section 2 was employed to establish the possible variations of eruption rates by varying the magma viscosity. It should be stressed that the magma viscosities given in Table 1 were computed from a laminar flow model where the flow is driven by the density contrast between the country rock and magma and an assumed flow velocity of about 1 m/s.

The magma viscosity depends strongly on its silica, dissolved water, and crystal contents. Dacites have a large silica content and, therefore, strong SiOSi bridging bonds which produces large viscosity (Hess, 1989). An addition of water to dacite depolarizes or replaces these strong bonds by much weaker SiOH bonds which effectively decrease the viscosity. The presence of crystals increases, however, the magma viscosity, and the combined effects of crystals and water content Y may be expressed by an equation of Shaw (1969), i.e.

$$\mu_L=\mu_{Lo}(1-1.35\phi)^{-2.5}e^{-133Y}=\mu_o e^{-133Y} \tag{47}$$

where ϕ is the volumetric fraction of crystals and μ_{Lo} is the viscosity of an anhydrous and crystal-free magma. Andesites and dacites in eruption have viscosities ranging from 10^4 to 10^{10} Pa-s. For the May 18, 1980 eruption and based on laminar flow models as noted above, Carey and Sigurdsson (1985) estimated a magma viscosity of 2.3×10^5 Pa-s based on the water content of 4.6% and crystal content $\phi=0.4$, whereas Scandone and Malone (1985) estimated a value of 2.2×10^6 Pa-s. As water exsolves due to pressure decrease along a conduit, Eqn. (47) predicts an order of magnitude increase in the magma viscosity. This increase, combined with the volumetric gas fraction increase, produces a rapidly increasing viscosity of the bubbly mixture (Eqn. 24) as the magma fragmentation region or maximum bubble packing density is approached. The assumption of a constant magma viscosity in a model reflects, therefore, only an average value of the viscosity in single phase and bubbly regions. The results in Figures 8–11 below were generated with constant and variable magma viscosities to assess the relative importance of this effect. In addition to the parameters indicated in Table 1 for computations it was also assumed that $K=0.03$ (smooth entrance), $N=10^{11}$ m^{-3}, and $d_f=50$ μm.

Figure 8 illustrates the distributions of critical discharge rates, exit pressures and velocities with the *average* magma viscosity and two different values of magma chamber pressures (185 and 265 MPa). The results in this figure are limited by the lower and upper bounds of the May 18, 1980 plinian eruption rates of Mt. St. Helens (10^7 and 4.4×10^7 kg/s), and are computed assuming that the discharge is critical. The mass discharge rates and exit pressures are strong functions of the average magma viscosity feeding the volcanic conduit which is between 10^6 and 10^7 Pa-s for the possible uncertainty of the magma chamber pres-

TABLE I

Parameters of the May 18, 1980 eruption of Mt. St Helens compiled from different sources for the plinian eruption phases. The last column in the table lists the input parameters for input to the nonequilibrium model.

Variable	Scandone and Malone (1985)	Carey and Sigurdsson (1985)	Rutherford et al. (1985)	Carey et al (1990)	Selected for comput
Magma type	dacite	dacite	dacite	dacite/andesite	dacite
Max. dis. water cont. [wt.%]	4 6	4 6	4 6±1	–	4 6
Magma density [kg/m^3]	2500	2600	–	–	2600
Crystal content [vol.%]	30–40	40	40	40	40
Country rock density [kg/m^3]	2700	2700	–	–	2700
Magma temperature [°C]	–	920–940	920–940	–	930
Magma viscosity [Pa-s]	$2.2\times10^{6(1)}$	$2.3\times10^{5(2)}$	–	–	(4)
Depth of magma chamber [km]	7–9	7–10	7.2±1	–	(4)
Magma confining pres. [MPa]	185–228(3)	190–250	190–250	–	(5)
Average conduit diameter [m]	100	95	–	–	95
Vent diameter [m]	–	<105–135	–	–	95
Magma discharge rate [kg/s]	$1\ 5\times10^7\pm40\%$	1.94×10^7	–	$10^7/4\ 4\times10^7$	(5)
Total discharge rate [kg/s]	–	2.28×10^7	–	–	(5)
Estimated min/max vel. [m/s]	–	200/330	–	–	(5)
Pumice volumetric frac. [%]	–	74	–	–	75
Degasing after magma fragm	–	yes	–	–	yes
Solubility constant [Pa$^{-0.5}$]	–	–	–	–	4.1×10^{-6}
Exponent, n	–	–	–	–	0.5
Friction coef. B_2	–	–	–	–	(4)

(1)Based on a laminar magma flow due to the buoyancy contrast of 200 kg/m^3 and velocity of 0.6 m/s
(2)Based on a laminar magma flow due to the buoyancy contrast of 100 kg/m^3 and velocity of 1 m/s.
(3)Based on the country rock density, conduit length, and atmospheric pressure, $\rho_c gL+P_{atm}$.
(4)Variable parameter in the model
(5)Result from the model

sure or conduit lengths. The magma chamber pressures were computed assuming a lithostatic pressure head with a country rock density of 2700 kg/m^3 and conduit lengths of 7 and 10 km. As shown in Figure 8, low discharge rates and exit pressures can be produced by high magma viscosities, such as a mafic dacite containing a high crystal content and discharged from the upper regions of the magma chamber during the initial and final eruptive sequences of the volcano as suggested by Carey et al. (1990). A lower magma viscosity produces higher discharge rates and is consistent with the eruption of silicic andesite during the intermediate eruption sequence of the May 18, 1980 eruption of Mt. St. Helens. This eruption sequence also produces the largest exit pressure. The smallest eruption rate of 10^7 kg/s produces an exit pressure close to the atmospheric and is consistent with the initiation and termination of the eruptions.

The gas and particle/droplet velocities at the conduit exit are not strongly affected by the magma viscosity, but do show an increase of the disequilibrium between the phases with an increasing viscosity or decreasing eruption rate. It is also seen from Figure 8 that the particle/droplet velocity is about 170 m/s whereas that of the gas exceeds 400 m/s. This produces a *mean* two phase flow velocity at the exit ranging from 150 to 185 m/s, and is computed from the discharge rates of 6208 and 1410 kg/m^2-s and mean densities ρ_m of 34 and 9.3 kg/m^3,

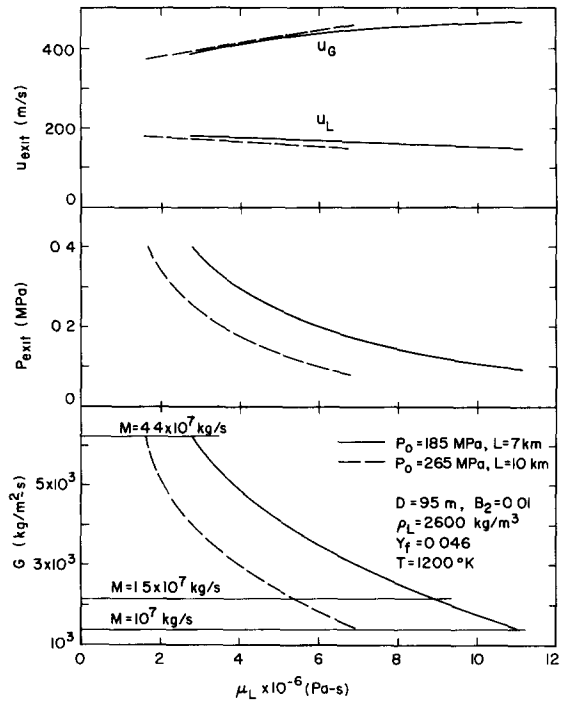

Fig. 8. Distributions of the critical discharge rates, exit pressures, and exit velocities with the average magma viscosity at different magma chamber pressures and conduit lengths for the Mt. St. Helens eruption on May 18, 1980. The parameters in the model are listed in Table 1.

respectively. The mean density is computed from:

$$\rho_m = \alpha\rho_G + (1-\alpha)\rho_L \tag{48}$$

Based on the plinian eruption column modeling (Wilson, 1976), Carey and Sigurdsson (1985) estimated that the range of exit velocities for the eruption of Mt. St. Helens is between 200 and 300 m/s. This velocity range is higher than the *mean* velocity range computed above but below the computed exit gas velocities of about 400 m/s.

Figures 9–11 illustrate the distributions of void fraction, pressure, and velocities along the conduit for different eruption rates, conduit lengths, and constant and variable magma viscosities. The volumetric fraction and pressure distributions in Figures 9 and 10 are significantly different in the bubbly and gas-particle/droplet flow regimes. The void fraction increase in bubbly flow produces a significant pressure gradient which rapidly increases as the magma fragmentation zone at $\alpha=0.75$ is approached due to the rapid increase of two-phase flow viscosity. The fluid pressure falls significantly below the lithostatic pressure and has a similar behavior for different discharge rates of Mt. St. Helens eruption (2160 and 6208 kg/m^2-s or 1.5×10^7 and 4.4×10^7 kg/s). The effect of allowing for the variable magma viscosity in the model according to Eqn. (47) is to produce a smaller pressure decrease below the lithostatic pressure and a much more steeper pressure and void fraction gradients close to the magma fragmentation zone than in the case of constant viscosity. The distributions in Figure 9 ($L=7$ km) and Figure 10 ($L=10$ km) are similar, and the pressure in the gas-particle/droplet flow regime recovers and exceeds the lithostatic pressure only in the proximity of the conduit exit. The inserts to the right of Figures 9 and 10 illustrate in more detail the local distributions of pressure close to the conduit exit.

The large difference between the lithostatic and fluid pressures in the vicinity of the magma fragmentation zone can lead to the rupture of the conduit wall and is consistent with the suggestion of Barberi et al. (1988) that phreatomagmatic eruptions occur due to water pouring into conduits and mixing with fragmented magma. The phreatomagmatic eruption of the Mt. St. Helens volcano occurred *before* the initiation of the first plinian phase and may have been caused in part due to the rupture of the conduit wall soon after the magma flow produced a large difference between the lithostatic and fluid pressures, causing the emptying of the underground aquifers. Wilson and Head (1981) suggest that the largest pressure differences are expected in the intermediate levels of the crust, whereas the lowest occur in the deep crust where rocks can deform plastically, and in the unconsolidated near-surface layers. The ultimate strength of rocks can vary significantly with water content in their pores, pres-

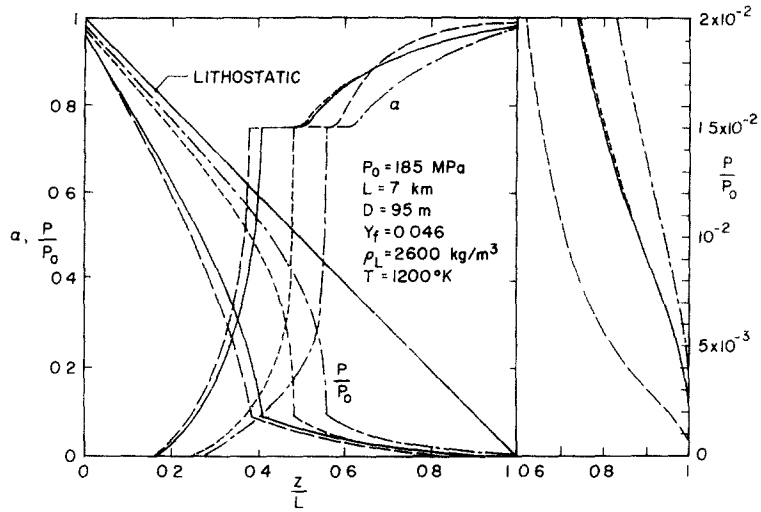

Fig. 9. Distributions of volumetric fraction and pressure along a conduit 7 km log and 95 meters in diameter for the Mt. St. Helens eruption on May 18, 1980. The results show the effects of critical discharge rates, constant and variable magma viscosities, and different values of the friction loss coefficient B_2. $G=6208$ kg/m^2-s: — μ_L=constant, $B_2=0$ 01. - - - μ_o=constant, $B_2=0.01$; —·— μ_o=constant, $B_2=0.1$ $G=2160$ kg/m^2-s· - - - μ_L=constant, $B_2=0.01$

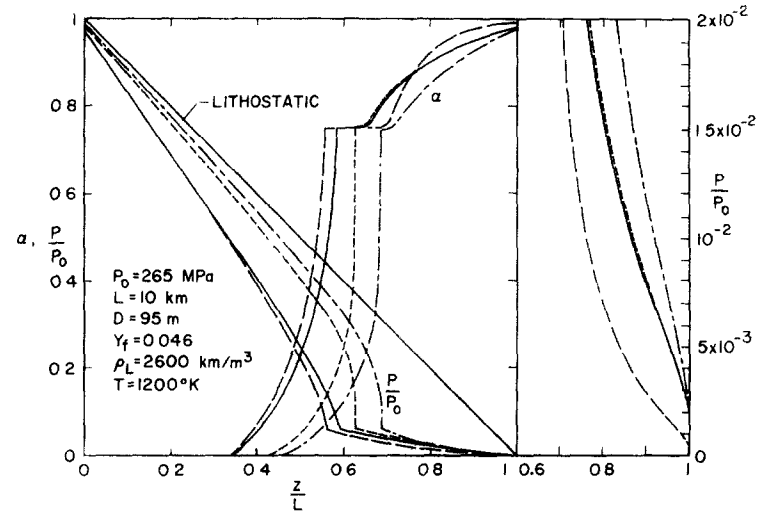

Fig. 10. Distributions of volumetric fraction and pressure along a conduit 10 km long and 95 m in diameter for the Mt. St. Helens eruption on May 18, 1980. The results show the effects of critical discharge rates, constant and variable magma viscosities, and different values of the friction loss coefficient B_2. The description of different curves is given in Fig. 9.

sure, and temperature, and its range is 40–300 MPa for andesite, 30–600 MPa for basalt, and 150–1000 MPa for granite (Carmichael, 1989). The failure criterion of a rock is a relationship between the principal effective stresses, representing a limit beyond which instability or failure occurs. According to one failure criterion, a failure initiates as soon as the minimum principal stress component reaches the tensile strength of the material, and the fracture normally aligns itself perpendicularly to the minimum principal stress component (Economides and Nolte, 1989). Both the elastic properties of rocks and tectonic forces

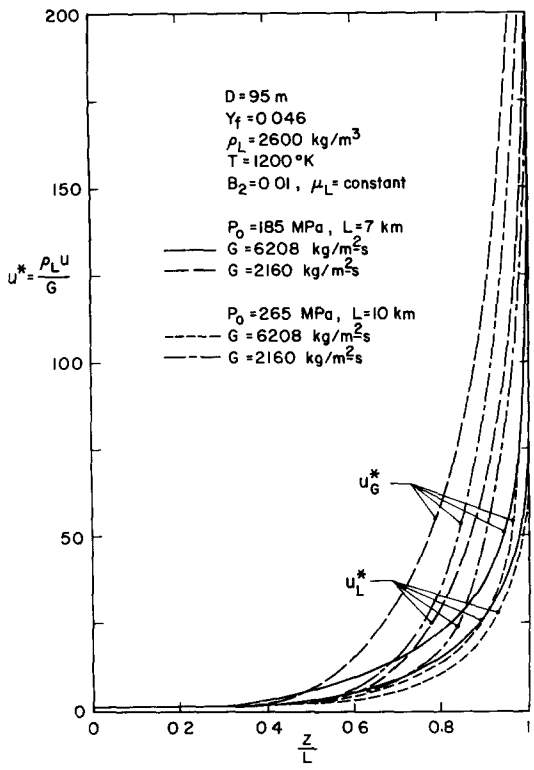

Fig. 11. Variations of gas and particle/droplet velocities along a 95-m-diameter conduit of the Mt. St. Helens eruption on May 18, 1980, with different critical discharge rates and conduit lengths.

are responsible for producing a horizontal stress on rocks at depths which when added to the difference between the lithostatic and fluid pressures in a conduit should exceed the fracture stress of the rock to produce a wall rupture. In Figure 9 and 10 the maximum predicted difference between the lithostatic and fluid pressure is about 90 MPa for the constant magma viscosity case, 80 MPa for the variable viscosity case, and 65 MPa for the variable viscosity and ten-fold increase in the turbulent friction coefficient ($B_2=0.1$). Upon comparison with the ultimate strength of rocks as given above, it follows that the predicted pressure differences may be too large and that some model parameters may not be very realistic. The pressure differences at the conduit inlet in Figures 9 and 10 reflect the losses associated with the flow acceleration and friction.

The extent of the disequilibrium between the phases in the gas-particle/droplet flow regime is reflected in the local distributions of velocities as shown in Figure 11. This disequilibrium is largest for the higher viscosity magmas, and the high exit gas velocities (in excess of 400 m/s) can transport high into the atmosphere very small (sub- and micron-size) pyroclasts.

3.3 The eruption of Vesuvius in AD 79

On August 24 at 1 p.m. in AD 79 a plinian eruption column began forming over Vesuvius and it was preceded by a phreatomagmatic explosion that generated the eruption cloud. For the next 7 hours, a phonolitic magma (white pumice) was ejected and the discharge increased to about 10^8 kg/s. After seven hours of plinian activity, or at about 8 p.m., the magma composition changed to the mafic phonolite (grey pumice) with the magma discharge rate increasing to about 1.5×10^8 kg/s at 1 a.m. on August 25. At this time the first of the six pyroclastic surges and flows were produced, obliterating in the first surge Herculaneum and in the fourth surge at 7:30 a.m. Pompei and killing about 2000 people (Sigurdsson et al., 1985, 1990; Carey and Sigurdsson, 1987).

The variation of the eruption rate of Vesuvius parallels the variation of physical and chemical composition of magma feeding the volcanic conduit. The eruption of white pumice is associated with the withdrawal of low density and viscosity evolved magma from the top of the magma chamber, whereas the eruption of grey pumice is associated with tapping of magma from the lower regions of the magma chamber. This magma was denser, contained less volatiles, was more viscous, and included larger proportions of crystals than the topping magma (see Table 2). Carey and Sigurdsson (1987) associate the vent widening during the eruption with the variation of the eruptive parameters of magma, whereas Sheridan et al. (1981) argue that the vent widening, or increase in the "explosivity" of the volcano, can

TABLE 2

Parameters of the AD 79 eruption of Vesuvius as compiled from different sources for the plinian eruption phases. The last column in the table lists the input parameters to the nonequilibrium model. The parameters during the initial and intermediate eruptions are separated by a slash.

Variable	Sigurdsson et al (1990)	Carey and Sigurdsson (1987)	Sigurdson et al (1985)	Barberi et al. (1981)	Selected for comput
Magma type	phonolite	phonolite	phonolite	phonolite	phonolite
Max dis. water cont. [wt.%]	4.7/3.5±0.5	high/low	high/low	-	4.7/3.5
Magma density [kg/m^3]	2380/2510	-/higher	2500/higher	2200/2600	2400/2550
Crystal content [vol.%]	-	18/40	-	-	18/40
Country rock density [kg/m^3]	-		-	2700	2700
Magma temperature [°C]	-	800	-	850	850
Magma viscosity [Pa-s]	2.2×10^{4}[1]/higher[2]		-	-	[4]
Depth of magma chamber [km]	-		>3	3–5	
Magma confining pres. [MPa]	-		-		132.54[3]
Average conduit diameter [m]	-	widens	-	-	[4]
Vent diameter [m]	-	=cond. dia.	160/260	-	cond. dia
Magma discharge rate [kg/s]	-	-	-	-	=total rate
Total discharge rate [kg/s]	8×10^{7}/1.4×10^{8}	8.2×10^{7}/1.5×10^{8}	10^{8}/1.5×10^{8}	-	8×10^{7}/1.5×1
Estimated min/max vel [m/s]	-	-	330/400		
Pumice volumetric frac. [%]	-	0.75	-		0.75
Degassing after magma fragm	-		-	-	[5]
Solubility constant [Pa$^{-0.5}$]	-	-	-	-	4.1×10^{-6}
Exponent, n	-		-	-	0.5
Friction coef. B_2	-	-	-	-	0.01

[1]Determined from chemical composition, crystal content, and temperature. The temperature and water content are not given.
[2]Due to higher crystal content
[3]Determined from country rock density, conduit length, and atmospheric pressure, $\rho_c gL + P_{atm}$
[4]Variable parameter in the model
[5]Result from the model.

also be affected by the interaction of water with magma.

Table 2 summarizes the available information of the plinian eruptions of Vesuvius in AD 79 that can be used to establish the lacking data and determine the local variation of flow parameters within the conduit. For each available parameter for which the information is known, Table 2 lists two values: the first pertaining to the early plinian phase and the second to the intermediate plinian phase where magma discharge was maximum and drawn from the deeper regions of magma chamber. The last column in the table summarizes the input parameters to the model on the basis of which it is possible to establish the variations of conduit diameter, exit pressure, exit velocities, etc., as a function of magma viscosity. The magma viscosity varies greatly as water exsolves along the conduit and considerably affects the results as discussed above for the eruption of Mt. St. Helens. The actual variation of magma viscosity with crystal content and water is unknown for the eruption of Vesuvius in AD 79 and was assumed to follow Eqn. (47). Moreover, it was also assumed that the exsolution law for rhyolite remains valid, and that $N=10^{11}$ m^{-3}, $d_f=50$ μm, $K=0.03$, and $B_2=0.01$. The results of computations are summarized in Figures 12–15.

Figure 12 illustrates the variations of conduit diameter, exit pressure, and exit gas and particle/droplet velocities for two different critical discharge rates (8×10^7 and 1.5×10^8 kg/s) with the *anhydrous* magma viscosity μ_o that includes the crystal content. It should be noted that the magma which produced the lower discharge rate contains a higher water content and is less denser than the magma which produced the highest eruption rate (see Table 2). For a fixed discharge rate, magma density, maximum dissolved water content, and a fixed length of conduit, larger diameter conduits can transport more viscous magmas (Fig. 12a) and create larger viscous pressure drops which is reflected in the lower exit pressures (Fig. 12b). For a fixed viscosity μ_o, larger magma discharges require larger conduit diameters and produce smaller exit pressures. The withdrawal of a more viscous magma from the magma chamber also produces a larger disequilibrium between the phases as reflected in the larger relative velocity between gas and pyroclasts (Fig. 12c).

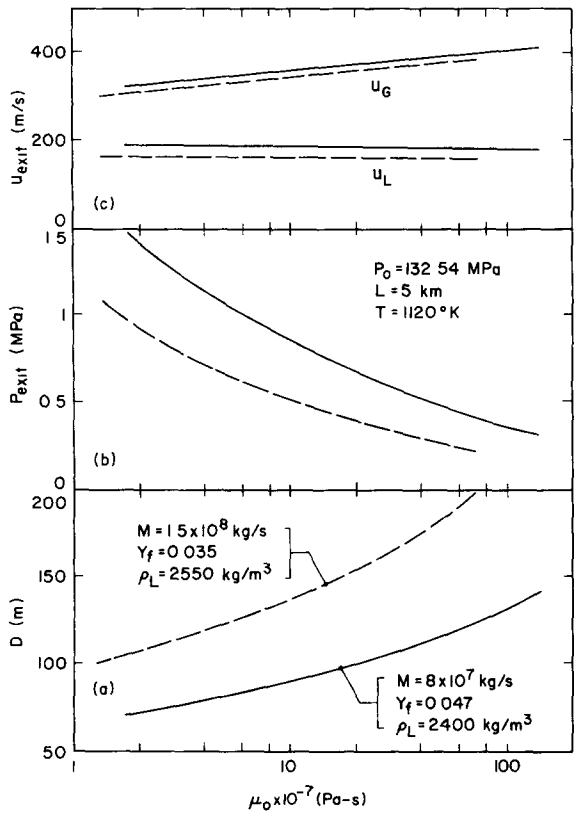

Fig. 12. Distributions of the conduit diameter, exit pressure, and exit velocities with the anhydrous magma viscosity and discharge rates for the eruption of Vesuvius in AD 79. The parameters in the model are listed in Table 2.

Figure 13 illustrates the distribution of the local volumetric fraction and pressure along the conduit for a conduit diameter of 100 m and two discharge rates. From these results it may be inferred that the earlier or first plinian eruption phase of Vesuvius was more prone in interacting with water from the underground aquifers than the intermediate eruption with maximum discharge, since it may have produced a larger difference between the lithostatic and fluid pressures. The phreatomagmatic explosion of Vesuvius before the establishment of the first plinian phase is, of course, an established fact (Sigurdsson et al., 1985) and reinforces the modeling conclusion which predicts a large difference between the lithostatic and fluid pressures immediately after the generation of the eruption cloud, having the potential to cause the conduit wall rupture and water inflow. This conclusion can also be reinforced by referring to Figure 14 where it is shown that an increase of conduit diameter, as may be caused by an increasing discharge rate, effectively decreases the difference between the lithostatic and fluid pressures, but not as much as in the case when the conduit diameter is maintained constant. The motion of the magma fragmentation zone along the conduit and conduit erosion, caused by the changes in the magma properties feeding the conduit, may thus also explain the activation of underground aquifers and intermittent phreatomagmatic explosions which can produce pyroclastic flows during the withdrawal of mafic phonolite from the magma chamber of Vesuvius. Note also in Figures 13 and 14 that the maximum water content of 4.7 wt.% during the magma withdrawal from the upper regions of the magma chamber produces exsolution near the conduit entrance and greater

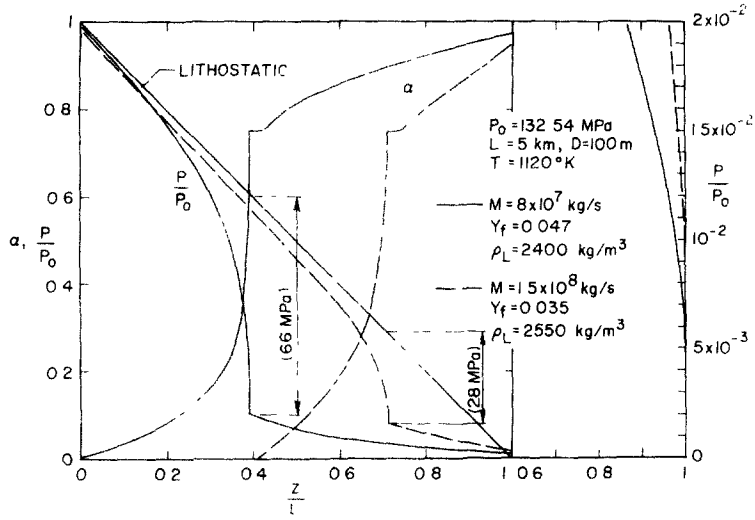

Fig. 13 Distributions of volumetric fraction and pressure along the 5-km-long conduit for the eruption of Vesuvius in AD 79, with a conduit diameter of 100 m and different discharge rates and water contents in magmas

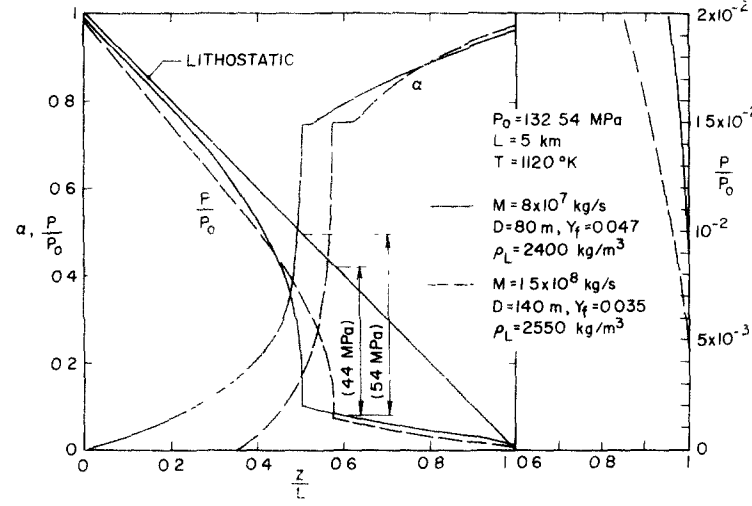

Fig. 14. Distributions of volumetric fraction and pressure along the 5-km-long conduit for the eruption of Vesuvius in AD 79, with conduit diameters of 80 and 140 m

depths where magma fragments. The inserts to the right in these figures provide an expanded view of the pressure distributions close to the conduit exit. The local variations of gas and particle/droplet velocities for the results in Figures 13 and 14 are presented in Figure 15, showing considerable disequilibrium between the phases in most of the conduit when magma contains large quantities of water.

The results in Figures 13–15 pertain to a 5-km-long conduit. A shorter conduit and a dissolved water content of 4.7% requires exsolution in the magma chamber and can produce two-phase flow at the conduit entrance during an eruption. Whether this scenario is likely or not cannot be ascertain from the available data, but it may have to be considered in the future modeling efforts of Vesuvius before using the model for the prediction of volcanic hazards.

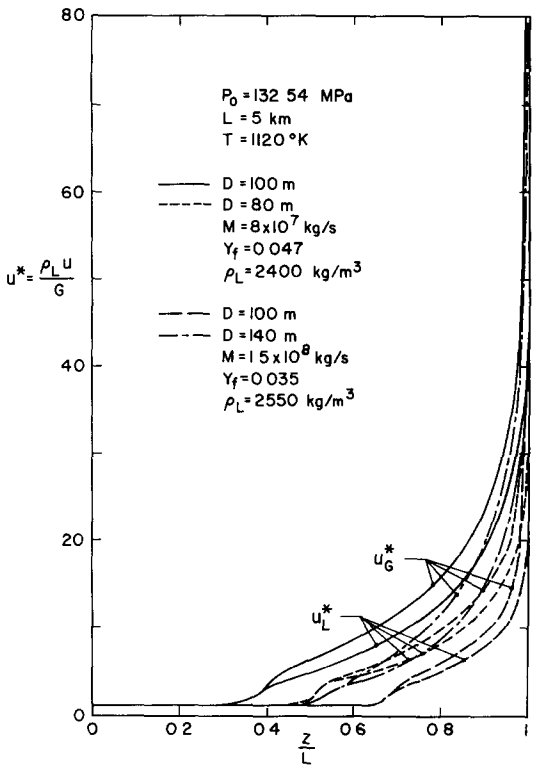

Fig. 15 Variations of velocities along the 5-km-long conduit for the eruption of Vesuvius in AD 79, with different conduit diameters and discharge rates.

4. Discussion

The results of one-dimensional and isothermal two-phase flow modeling in volcanic conduits presented in the previous section demonstrate the importance of nonequilibrium effects as affected by the magma viscosity. The exsolution of a hydrous magma produces an increasing two-phase flow viscosity along the conduit for two reasons: first because the liquid becomes more viscous and its particles move with more difficulty relative to each other, and second the liquid flows with more difficulty between the growing bubbles. This increasing flow resistance produces a large frictional pressure drop close to the maximum packing density of bubbles in the liquid, leading to the magma fragmentation and change of the flow regime to the one with a continuous gas phase with dispersed particles and droplets. The large difference between the local lithostatic and fluid pressures in a conduit in the proximity of the magma fragmentation zone can produce a failure of the conduit wall, cessation of the eruption due to the conduit closure, or an inflow of water into the conduit through the fractured wall. This implies that upon the establishment of a flow or an eruption there should be a high probability of producing phreatomagmatic explosions as the underground aquifers are emptied. The phreatomagmatic explosions are known to occur before and during the eruption of Mt. St. Helens in 1980 and Vesuvius in AD 79 (Sigurdsson et al., 1985; Carey et al., 1990). The more viscous the magma the larger will be the difference between the lithostatic and fluid pressures in the conduit near the magma fragmentation zone and, therefore, the higher will be the probability of phreatomagmatic eruptions and changes of the eruptive modes of a volcano as magma is tapped with different physical properties from different regions of a magma chamber. A large viscosity magma produces a large frictional pressure drop before magma fragments which is responsible for the large pressure difference between lithostatic and fluid pressures.

The widening of a conduit during an eruption can be associated with the dissipation of energy of the fluid at the conduit wall and variation of physical and chemical characteristics of magma which feeds the conduit. The viscous dissipation of fluid is greater for greater viscosity magmas which should in turn produce larger conduit erosion rates. The withdrawal of magma with different properties (density, anhydrous viscosity, crystal content, water content, etc.) can produce a change in the location of the magma fragmentation zone and different erosion rates in different parts of a conduit. A magma/water interaction can produce a rapid vaporization of water and va-

por pressure increase leading to the creation of high velocities and large dissipation of fluid energy at the wall. A large conduit wall erosion rate can produce a dense two-phase mixture at the conduit exit and contribute towards the eruption column collapse, producing pyroclastic flows and surges.

The maximum predicted differences between the lithostatic and fluid pressures in the conduits for the eruptions of Mt. St. Helens in 1980 and Vesuvius in AD 79 may be too large and not very realistic due to the possibility of large variation of rock properties and tectonic forces in volcanic edifices of these volcanoes. By assuming that the conduit wall is made up of a solidified magma which initially penetrated or slowly percolated upwards towards the surface before the opening of the volcanic vent, it is possible to argue that the predicted maximum pressure differences in the conduits of Mt. St. Helens and Vesuvius do not exceed the allowable ultimate stress limits of rocks (Carmichael, 1989) at intermediate depths where the fracture stresses of rocks are the greatest (Wilson and Head, 1981). The predicted locations of these maximum pressure differences or magma fragmentation zones all lie at intermediate depths of the conduits (see Figs. 9,10,13,14).

If the limits of the rock fracture stresses and locations of aquifers can be ascertained in different regions of a volcanic system then it may be possible to employ the above nonequilibrium model for determining a consistent or corresponding set of flow parameters and mass discharge rates. If this is accomplished it may turn out, for some combination of parameters, that the conduit cannot sustain a critical or maximum flow and that the conditions surrounding the volcanic vent determine the flow in the conduit. Moreover, the closing of a volcanic eruption cannot only be associated with the reduction of stagnation or driving pressure for magma in a magma chamber, but also with the conditions above the vent, the structure of the volcanic edifice, and with the properties of magma feeding the conduit. This would then imply that the flow in the conduit can be determined only by simulating the behavior of the entire volcanic system. A global simulation of volcanic transport processes would be the ultimate objective of volcanic modeling efforts and may lead to the prediction and control of volcanic hazards (Dobran et al., 1990).

For the plinian eruptions of Mt. St. Helens on May 18, 1980 and Vesuvius in AD 79, the predicted exit pressures are always greater than the atmospheric pressure, and the exit velocities can reach several hundred meters per second (Figs. 8, 12). These predictions are based on the constant diameter conduits and do not allow for vent flarring which is normally expected during the eruptions due to the unconsolidated nature of rocks close to the surface. The vent flarring should be, therefore, a complicated function of the local rock structure, properties of the two-phase mixture in the conduit which contribute towards the dissipation of energy and wall erosion, and properties of the local atmosphere and topography of the surface of volcano. Some of these effects can be easily incorporated into the model and are left for future studies. The predicted gas velocities (up to 500 m/s) are sufficiently large and capable of producing the thrusting of pyroclasts and lithics high into the atmosphere. The height of an eruption cloud can be well predicted by the mass eruption rate and temperature difference between the magma and atmosphere (Wilson et al., 1978; Sparks, 1986; Woods, 1988), whereas the conditions determining the plinian or collapsing columns appear to be determined principally by exit pressure and Richardson number defined as (Valentine and Wohletz, 1989):

$$Ri=\frac{\rho_m u_{exit}^2}{g(\rho_m-\rho_{atm})0.5D_{vent}} \tag{49}$$

where ρ_m is the mean two-phase flow density at the conduit exit. The conditions leading to the rising (large Ri) and collapsing (small Ri) columns should be more complicated than

those expressed by Eqn. (49), and the relative velocity between the phases and the size of pyroclasts and lithics should also play an important role. The modeling of pyroclastic dispersions above the volcanic vents requires an accurate knowledge of two-phase flow boundary conditions at the exit of the vent which must be determined from accurate modeling of nonequilibrium flow in volcanic conduits.

5. Summary and conclusions

A nonhomogeneous, steady-state, isothermal, and one-dimensional two-phase flow model was developed for modeling flows in volcanic conduits. The model incorporates the relative velocity effect between the phases and accounts for the magma viscosity increase as the dissolved gas is exsolved along a conduit. The resulting set of nonlinear differential equations was solved numerically by a stiff numerical solver which is very robust and was effectively implemented on a personal computer. The predictions of the model were first tested by comparing the results with basaltic fissure eruptions obtained by a homogeneous model. The predicted results from the nonequilibrium model are in excellent accord with the homogeneous model in the limit of constant magma viscosity and very large interfacial drag which prevents the relative motion between the phases. The sensitivity analysis of several modeling parameters demonstrated a minor effect on the predicted flow parameters in the conduits. Employing the parameters of the eruptions of Mt. St. Helens on May 18, 1980 and Vesuvius in AD 79, the model was used to determine the possible variations of magma properties and conduit geometries during these eruptions.

The numerical results show that large viscosity magmas can produce a large difference between the lithostatic and fluid pressures in the proximity of magma fragmentation in a conduit. This pressure difference can produce the conduit wall fracture, closure of the volcanic vent, or inflow of water into the conduit through the fractured wall from underground aquifers. Such a large pressure difference can occur in different parts of the conduit, depending on the properties of magma which feeds the conduit. The motion of the magma fragmentation zone along a conduit during the course of an eruption may also cause intermittent disruption of the plinian eruption phases as caused by the phreatomagmatic explosions due to the activation of aquifers at different depths. These explosions and the variation of magma properties and pressure at the conduit entrance may produce a significant wall erosion due to the high energy dissipation of very viscous magmas. By increasing the magma viscosity produces lower exit pressures and larger disequilibrium effects at the exit of a conduit. The predicted exit velocities for the Mt. St. Helens and Vesuvius eruptions range from about 200 m/s for the particle/droplet phase to 500 m/s for the gas phases, without accounting in the model for vent flarring as normally required by a homogeneous model in order to predict large exit velocities. The homogeneous model is not adequate for the prediction of critical mass flow rates from small fissure widths and for large viscosity magmas, and can produce considerable errors in the distributions of local flow parameters in and at the exits of conduits. The viscosity of magma in a magma chamber has a overwhelming influence on the flow distribution along a conduit and the maintenance of eruptions, and much effort needs to be made in the future to identify this parameter, either experimentally or through simulations of magma chamber processes.

The results of the present modeling effort point to a great need in identifying the rock structure and location of aquifers of volcanic edifices. Without such a quantitative identification it may be futile to carry out the conduit modeling for the purpose of assessing the volcanic hazards. With this information and accurate knowledge of the properties of magma feeding a volcanic conduit, it may then be pos-

sible to establish the necessary conditions at the volcanic vent for input into a model of pyroclastic dispersions. The future work in volcanic conduit modeling should include nonisothermal flow, conduit wall erosion, interaction of magma with water, transient nonequilibrium two-phase flow, and volcanic structure–fluid interactions.

References

Barberi, F., Bizouard, H., Clocchiatti, R., Metrich, N., Santacroce, R. and Sbrana, A., 1981. The Somma-Vesuvius magma chamber: a petrological and volcanological approach. Bull. Volcanol., 44: 295–315.

Barberi, F., Navarro, J.M., Rosi, M., Santacroce, R. and Sbrana, A., 1988. Explosive interaction of magma with ground water: insights from xenoliths and geothermal drillings. Rend. Soc. Ital. Mineral. Petrol., 43: 901–926.

Bruce, P. and Huppert, H.E., 1989. Thermal control of basaltic fissure eruptions. Nature, 342: 665–667.

Buresti, G. and Casarosa, C., 1989. One-dimensional adiabatic flow of equilibrium gas-particle mixtures in long vertical ducts with friction. J. Fluid Mech., 203: 251–272.

Carey, S. and Sigurdsson, H., 1985. The May 18, 1980 eruption of Mt. St. Helens 2. Modeling of dynamics of the plinian phase. J. Geophys. Res., 90: 2948–2958.

Carey, S. and Sigurdsson, H., 1987. Temporal variations in column height and magma discharge rate during the 79 A.D. eruption of Vesuvius. Geol. Soc. Am. Bull., 99: 303–314

Carey, S., Sigurdsson, H., Gardner, J.E. and Criswell, W., 1990. Variations in column height and magma discharge during the May 18, 1980 eruption of Mt. St. Helens. J.Volcanol. Geotherm. Res., 43: 99–112.

Carmichael, R.S., 1989. Physical Properties of Rocks and Minerals. CRC Press, Boca Raton, Florida.

Dobran, F., 1987. Nonequilibrium modeling of two-phase critical flows in tubes. J. Heat Transfer, 109: 731–738.

Dobran, F., Barberi, F. and Casarosa, C., 1990. Modeling of volcanological processes and simulation of volcanic eruptions. C.N.R.-Gruppo Nazionale per la Vulcanologia, Italy, Rep. VSG90-01

Economides, M.J and Nolte, K.G., 1989. Reservoir Stimulation. Prentice Hall, Englewood Cliffs, N.J.

Fast, J.D., 1972. Interaction of Metals with Gases. Barnes and Noble, New York, N.Y.

Giberti, G. and Wilson, L., 1990. The influence of geometry on the ascent of magma in open fissures. Bull. Volcanol., 52: 515–521

Hess, P.C., 1989. Origins of Igneous Rocks. Harward University Press.

Hindmarsh, A.C., 1983. ODEPACK, A systematized collection of ODE solvers. In: R.S. Stepleman (Editor), Scientific Computing. North Holland, Amsterdam

Ishii, M. and Zuber, N., 1979. Drag coefficient and relative velocity in bubbly, droplet and particulate flows AIChE J., 25: 843–855.

Kieffer, S.W., 1977. Sound speed in liquid–gas mixtures: water–air and water–steam. J. Geophys Res., 82: 895–904.

Kieffer, S.W., 1981. Blast dynamics of Mt. St. Helens on May 18, 1980. Nature, 291: 568–571

Macdonald, G.A., 1972. Volcanoes Prentice Hall, Englewood Cliffs, N.J

Pai, S.I., Hsu, Y. and O'Keefe, J.A., 1978. Similar explosive eruptions of lunar and terrestrial volcanoes. Proc 9th Lunar Planet. Sci. Conf., pp. 1485–1508.

Rutherford, M.J., Sigurdsson, H., Carey, S. and Davis, A., 1985. The May 18, 1980 eruption of Mt St. Helens 1. Melt composition and experimental phase equilibria J. Geophys. Res., 90: 2929–2947

Scandone, R. and Malone, S.D., 1985. Magma supply, magma discharge and readjustment of the feeding system of Mt. St. Helens during 1980. J Volcanol Geotherm. Res., 23. 239–262

Shaw, H.R., 1969. Rheology of basalt in the melting range. J. Petrol., 10: 510–535.

Sheridan, M.F., Barberi, F., Rosi, M. and Santacroce, R., 1981. A model for plinian eruptions of Vesuvius. Nature, 289: 282–285

Sigurdsson, H., Carey, S., Cornell, W. and Pescatore, T., 1985. The eruption of Vesuvius in AD 79, Nat. Geogr Res., 1: 332–387

Sigurdsson, H., Cornell, W. and Carey, S., 1990 Influence of magma withdrawal on compositional gradients during the AD 79 Vesuvius eruption Nature, 345: 519–521

Sparks, R.S.J., 1978. The dynamics of bubble formation and growth in magmas: a review and analysis J Volcanol. Geotherm. Res., 3: 1–37

Sparks, R.S.J., 1986. The dimension and dynamics of volcanic eruption columns. Bull. Volcanol., 48: 3–15.

Turcotte, D.L., Ockendon, H., Ockendon, J.R and Cowley, S.J., 1990. A mathematical model of vulcanian eruptions. Geophys. J. Int., 103: 211–217

Valentine, G.A. and Wohletz, K.H., 1989 Numerical models of plinian eruption columns and pyroclastic flows. J. Geophys. Res., 94. 1867–1887

Vergniolle, S. and Jaupart, C., 1986. Separated two-phase flow and basaltic eruptions. J. Geophys Res., 91 12,842–12,860.

Wallis, G.B., 1969. One-Dimensional Two-Phase Flow McGraw Hill, New York, N.Y.

White, F.M., 1979. Fluid Mechanics. McGraw Hill, New York, N.Y.

Wilson, J. and Head III, J.W., 1981 Ascent and eruption of basaltic magma on the earth and moon J. Geophys. Res., 86: 2971–3001

Wilson, L., 1976. Explosive volcanic eruptions, III. Plinian eruption columns. Geophys. J.R. Astron. Soc , 45: 543–556.

Wilson, L., Sparks, R.S.J., Huang, T.C. and Watkins, N.D., 1978. The control of volcanic column heights by eruption energetics and dynamics. J. Geophys. Res., 63: 1829–1835.

Wilson, L., Sparks, R.S.J. and Walker, G.P.L., 1980. Explosive volcanic eruptions, IV. The control of magma properties and conduit geometry on eruption column behavior. Geopys. J. R. Astron. Soc., 63: 117–148.

Woods, A.W., 1988. The fluid dynamics and thermodynamics of eruption columns. Bull. Volcanol., 50: 169–193.